ELSEVIER

Contents lists available at ScienceDirect

Results in Engineering

journal homepage: www.sciencedirect.com/journal/results-in-engineering



Research paper

Electrical equivalent circuit modeling of self-shielding DC high temperature superconducting cable considering the effect of fault on its electrothermal performance

Mohammad Ali Salehi, Seyyedmeysam Seyyedbarzegar * 0

Faculty of Electrical Engineering, Shahrood University of Technology, Shahrood, Iran

ARTICLE INFO

Keywords: Self-shielding DC HTS cable Electrical equivalent circuit model AC losses Transient state Current ripple

ABSTRACT

DC High temperature superconducting (HTS) cables have been considered from the point of view of very low losses and high current capacity. In order to properly utilize these cables in power systems, it is necessary to evaluate their electrothermal and magnetic performance in steady and transient conditions as well as in different power network structures. In this paper, a 1 kV 3 kA self-shielding DC HTS cable with a multilayer structure is modeled using the electrical equivalent circuit method (ECM) in MATLAB/SIMULINK. The current flowing through the tapes and layers, temperature and losses, as well as the magnetic field and critical current in different layers, according to the specific conditions of the self-shielding DC HTS cable, were investigated as important parameters in evaluating the steady and transient operation. In order to study the transient state in the power system, pole-to-pole and pole-to-ground faults were simulated for different fault resistances. In addition, the effect of AC ripple on the DC current entering the cable is considered as a factor affecting losses. The results show that under stable operation of power system, the current flowing through the forward and backward layers is equal. However, in transient conditions, the balance of current between the layers will be lost. Also, with the decrease in fault resistance, in addition to the increase in the current flowing through the layers and the imbalance between them, the temperature and losses show a significant increase. In some situations, the fault caused a change in the operating mode of the superconducting cable, which can be dangerous for the operation of the cable.

1. Introduction

Superconducting materials, which exhibit zero electrical resistance at low temperatures, have significant advantages in the electrical industry. One important application of superconductors is in the transmission of electrical energy through superconducting cables [1–3]. Superconducting cables are divided into two general categories: AC and DC. Although AC cables are widely used, DC superconducting cables have advantages over AC superconducting cables due to their frequency independence. These advantages include higher electrical energy transfer, flexible power regulation, and near-zero losses [4]. DC HTS cables are operated as part of the power system under steady-state and fault conditions [5]. In this regard, studies conducted on DC HTS cables can be examined in three categories. The first category is studies that investigate the experimental characteristics of superconducting cables under steady-state and transient conditions in a laboratory setting.

Although laboratory methods are reliable, they can be very costly and sometimes destructive if fault tests are repeated. The second category of studies uses numerical formulas that are solved by numerical methods such as finite element method (FEM). Modeling performed in this method is usually very slow due to their level of accuracy and requires powerful computing processors. In addition, modeling based on the FEM cannot be implemented for real-time applications and is often used in the design phase of a superconducting device. The third category conducted to describe the performance of DC HTS cables is the use of equivalent circuit models [6,7]. ECMs are faster than FEM and can provide high accuracy results. This method can model the thermal, electrical and magnetic properties of HTS cables very quickly. This condition allows these models to be used for online investigation of cables under different operation conditions. In this regard, in [8] the various parameters required in the design and modeling of DC HTS cables were described. Several case studies were conducted at different

E-mail address: seyyedbarzegar@shahroodut.ac.ir (S. Seyyedbarzegar).

^{*} Corresponding author.

Table 1Review of some research conducted in the field of modeling DC high-temperature superconducting cables.

Ref	Characteristics	Research Objective	Modeling Method	Results	weaknesses
[25]	Single-pole high- temperature superconducting cable, 100 kV, 10 kA	Fault study of an HVDC system using HTS DC cable and modular multilevel converters (MMC)	Cable modeling based on compact π model and HVDC system in PSCAD/EMTDC	* Transient study on HTS DC cable transmission line and a fault on the AC side * No quenching of HTS DC cable after pole-to-ground fault due to fault current being less than the critical cable current * Demonstration of the protective feature of HTS DC cable during pole-to-pole fault	*No magnetic analysis of the cable under steady and fault conditions. * No effect of parameters such as mutual inductance, twist angle and pitch, HTS strip circuit model in the design. * No investigation of the effect of current ripple and losses under fault conditions.
[26]	Multilayer DC HTS cable, 80 kV, 250 MW, 500 m	Investigation of current distribution and critical current of the cable under fault conditions	FEM and the circuit model of current distribution	* The need for a cross-sectional area larger than 240 mm to withstand the fault * Low impact of current imbalance in layers on cable thermal performance	*The superconducting strip resistance is constant throughout the fault and is unaffected by temperature and current density changes. * Not investigating the effect of current ripple and losses under fault conditions
[27]	Bipolar high temperature superconducting cable 3.6 kV 3 kA, 30 m	Comparing the characteristics of HTS DC cable with a conventional cable in fault conditions	Modeling a bipolar DC power system and the π model of the cable in MATLAB software	* Displaying the cable voltage waveform in fault conditions with different fault resistances	*Using the π model for HTS cable modeling and not considering mutual inductance, twist angle and twist pitch, strip circuit model * Not considering the effect of temperature and current density changes during the fault period * Not considering the ripple effect and not analyzing the magnetic and thermal behavior of the cable
[28]	High temperature superconducting HVDC coaxial cable, 100 kV, 1 GW	analysis of temperature, resistance, current distribution and losses parameters under normal and transient conditions	Distributed and compact volume element circuit model developed in MATLAB	*Fault current 22 kA * Temperature of HTS strips under fault conditions, 230°K * Recovery time 227 s	* Limitation on the faults considered for transient simulation * No magnetic analysis of the cable under fault conditions
[29]	High-temperature superconducting cable with cold dielectric	Investigating the effect of twist angle changes on magnetic flux density	3D finite element (3D FEM) in COMSOL	* Electrothermal and electromagnetic analysis	* No transient analysis * Cable quenching with increasing temperature

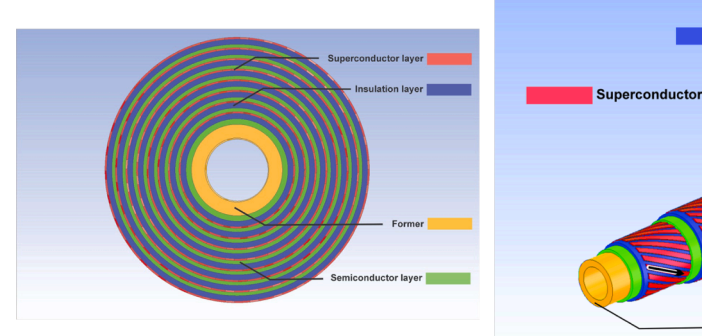
voltage levels and compared with conventional copper cables in terms of reduction of losses, economic efficiency, etc. Also, modeling of DC HTS cable and the effect of its different structures on critical current was studied in [9] to provide a basis for designing a practical DC HTS cable. Modeling of DC superconducting cable using a 3D electromagnetic model along with presenting different models of cable cooling system based on finite element method was another research conducted in this field and was discussed in [10]. The design process of DC HTS cables using commercial REBCO tapes was presented in [11], where the dependence of critical current density of superconducting tapes, thermal properties of materials and different cooling modes of the cable were investigated. The performance of DC HTS cable in different topologies of HVDC network as well as parallel connection with an AC network was analyzed in [12]. In this reference, a distributed parameter model based on the π model of the transmission line was used to model the cable. Selected model did not allow for the suitable investigation of the cable parameters from a superconducting perspective.

Investigating the performance of DC superconducting cables under steady-state conditions provides very useful information on the design conditions and electrothermal performance of the cable. However, modeling and studying the behavior of DC superconducting cables with the aim of considering the effect of fault parameters is necessary [13, 14]. The fault may be in the form of a short circuit between lines or line to ground in the AC side or a pole to pole or pole to ground fault in the DC side [15–16]. When a fault occurs, the current flowing in the HTS conductors exceeds the permissible value, which may lead to the cable change operation mod from superconducting to resistive state [17,18]. Generally, fault conditions significantly affect temperature rise [19], increase cable resistance, and alter the critical current during the fault. In this regard, the modeling parameters of DC superconducting cable were described in reference [20] and the transient study of DC HTS cable in a high-voltage power system with a voltage level of 100 kV was

carried out under different scenarios. Providing a suitable solution to investigate the tolerance level and recovery time of DC superconducting cable in a fault condition was investigated in [11]. In order to compare the studies conducted in design and modeling of DC high-temperature superconducting cables, the results and their strengths and weaknesses are presented in Table 1.

Another parameter affecting the performance of DC HTS cable is the physical structure. DC HTS cables are divided into single-core and double-core types. Meanwhile, single-core HTS DC cables can be divided into single-pole and coaxial double-pole types according to the conductors. In order to achieve higher current capacity in DC HTS cables, the conductors of these cables are designed as multilayers, in which a number of HTS tapes are twisted in parallel in each layer [21,22]. The results of the studies have shown that the current distribution of the cable layers is unbalanced due to the different self- and mutual inductance of the layers, which will lead to current imbalance in different layers [23,24].

In order to achieve uniform current distribution, a self-shielding DC HTS cable was used, which can eliminate the effect of the magnetic field of the layers and minimize the critical current of the tapes [30]. In this cable, the self and mutual inductances of the layers can be adjusted to achieve uniform current distribution by changing the angle and pitch of the winding [31]. In the self-shielding DC superconducting cable, the AC losses are greatly reduced compared to the conventional multilayer cable. By weakening the effects of the interlayer magnetic fields and the zero magnetic field in the external space, the critical current attenuation of the layers will be small and the current carrying capacity will be effectively increased [32]. In this regard, in [23] the self-shielding DC superconducting cable was modeled in two cases using the finite element model considering the effect of the current direction in the layers. Also, quench resistance according to electrothermal behavior of four-layer self-shielding DC HTS cable has been investigated in this



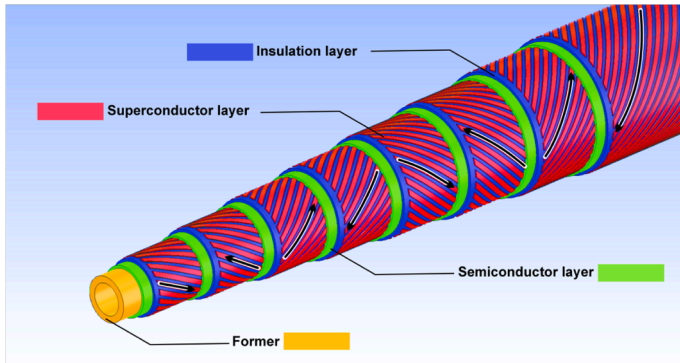


Fig. 1. Self-shielding DC HTS Cable structure.

Table 2Designed Cable Specifications.

Parameter	Quantity
Operating voltage	1 kV
Current capacity	3 kA
Frequency in AC side	60 Hz
Type of superconducting tape	YBCO
Thickness of tape	0.18 mm
Width of tape	2.5 mm
Critical temperature of tape	92 °K
Operating temperature of tape	77 °K
Critical current of tape	76 A
Type of electrical insulation	PPLP
Insulation thickness	$0.1 \times 2 \text{ mm}$
Former radius	9 mm
Cable structure	Multilayer coaxial bipolar (4 × 2 layers)
Cable length	1 m

paper. In [33], the self-shielding property of DC superconducting cable was analyzed and the transient characteristic of a voltage source converter during a pole-to-pole short-circuit fault was investigated [34].

Studies have shown that the research conducted in estimate the electromagnetic and thermal behavior of self-shielding cables under steady and transient conditions based on ECM has been very limited. Most of these researches focus on numerical models and finite element methods. Accordingly, the aim of this paper is to provide a circuit model of an eight-layer self-shielding DC high-temperature superconducting cable by considering full details of the parameters affecting its performance. In this regard, the electrothermal parameters such as current, temperature and losses of the modeled cable under steady conditions and single-pole and pole-pole faults have been evaluated. In addition, the evaluation of the magnetic field in the cable and its effect on the critical current as one of the important factors has been carried out. Fault resistance, as a parameter that causes current change, is another factor that has been investigated. Also, the effect of DC current ripple, which increases the AC losses of the cable, has also been evaluated.

2. The studied self-shielding superconducting cable

In multilayer HTS cables, the magnetic field produced by each layer becomes stronger with increasing current amplitude, which will reduce the critical current in each tape. It is obvious that when the cable transmits a large current, the reduction of the critical current will affect the capacity of the cable. Therefore, if the effect of the magnetic field is largely eliminated or reduced, it is possible that the capacity of the DC HTS cable can be significantly increased. Accordingly, the self-shielding HTS DC cable with a high current capacity was selected, which, due to the insulation limitations, is applicable to low voltage levels with an operating voltage of $<1~\rm kV$ [35]. The structure of this cable is shown in Fig. 1. Also, the specifications and design parameters of the cable are presented in Tables 2 and 3 [36]. The cable under study consists of 8 layers, where layers 1, 3, 5, and 7 are forward and layers 2, 4, 6, and 8 are backward conductors. The direction of current in the forward layers is indicated by 1 and in the backward layers by -1. Also, the direction of the twist of the tapes in each layer is indicated by the positive and negative signs.

3. Modeling

In this section, at first, the power system configuration and ECM model have been shown. Next, the modeling method and its considerations are described.

3.1. Circuit modeling of self-shielding DC HTS cable

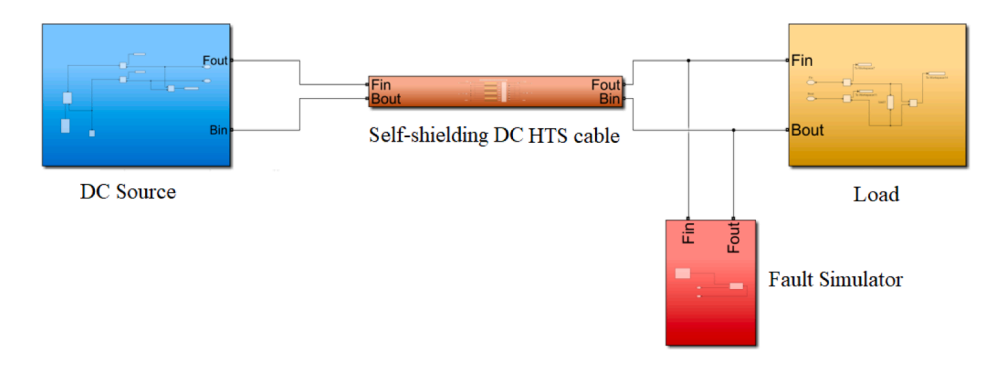
In this paper, the circuit model is implemented in MATLAB/SIMU-LINK software and the required values of the input parameters under steady and transient conditions are calculated and applied to the model. Accordingly, the values of output parameters such as current in different layers, magnetic field, AC losses and temperature can be extracted at any moment of the simulation time. In order to investigate the performance of the cable in the power system and implement different operating conditions, the cable model was placed in a system including a controllable DC power generation source, electrical load and fault simulator. The network configuration is shown in Fig. (2-a) and equivalent circuit model of a self-shielding DC HTS cable is shown in Fig. (2-b).

3.2. Circuit model parameters

Due to the AC ripple effect in the rectifier output, the HTS tape in this

Table 3Design Parameters of 8-Layer Self-shielding DC HTS Cable.

Layer number	Layer 1	Layer 2	Layer 3	Layer 4	Layer 5	Layer 6	Layer 7	Layer 8
Strip twist angle	16.5	22.6	13.4	20.2	11.1	18.5	11.7	18.3
Strip twist direction	+	+	-	_	+	+	_	_
Number of strips per layer	9	9	11	11	13	13	15	15
Flow direction per layer	1	-1	1	-1	1	-1	1	-1
Diameter of each layer in millimeters	9.6	10.8	12	13.4	14.8	15.6	16.8	18



(a)

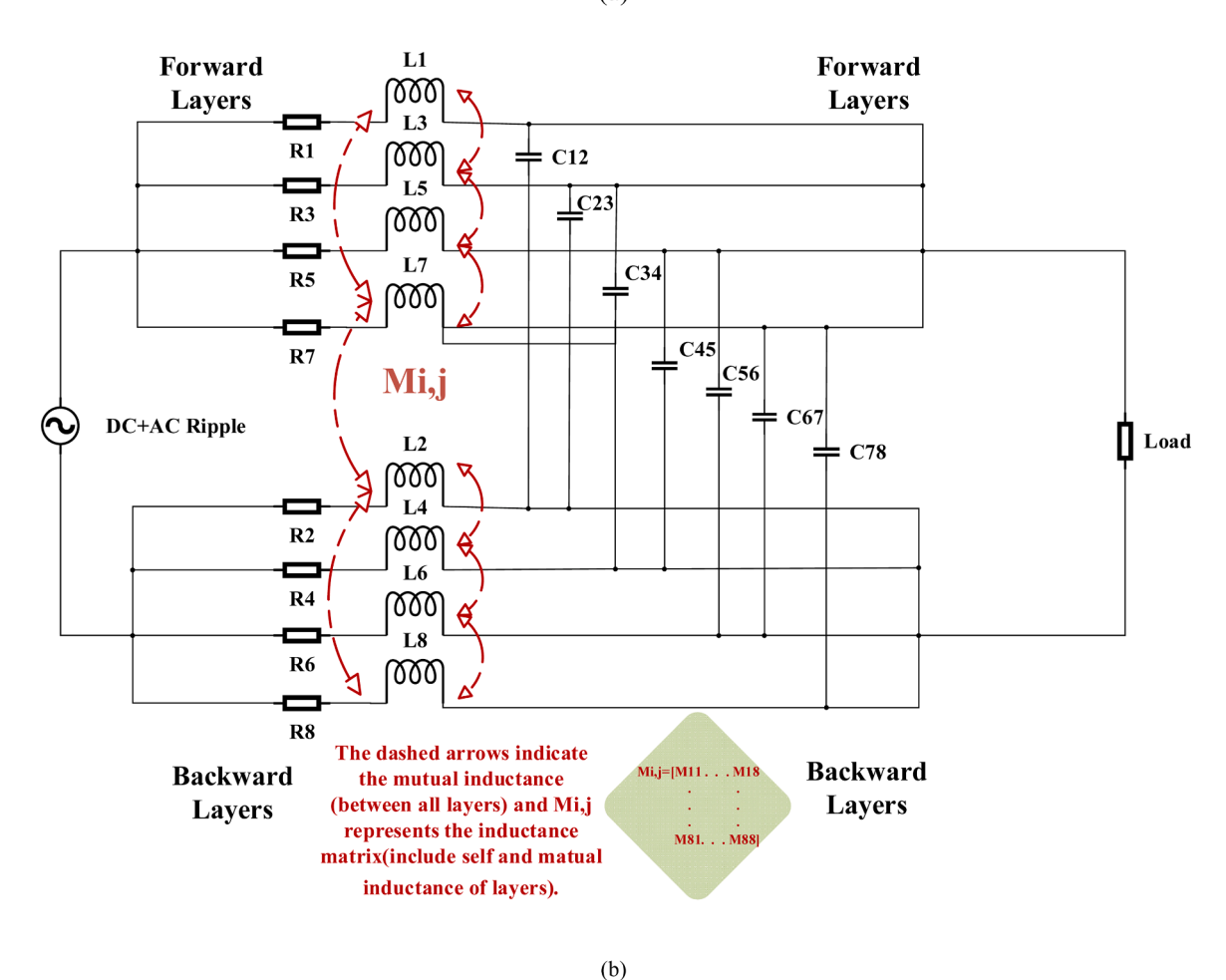


Fig. 2. Equivalent circuit model of simulated system, a) Power system circuit model b) HTS cable equivalent circuit model.

cable carries both DC and AC currents and is simultaneously affected by the magnetic fields caused by them. Therefore, due to the AC ripple effect in the cable conductor, it is necessary to model DC HTS cables with the AC HTS cable design principles.

In DC superconducting cables, each tape is exposed to magnetic fields caused by currents passing through other tape of the cable. The magnetic field has an axial and azimuthal component. These two components of the magnetic field act as parallel and axial fields with the tape, which are created by the currents flowing in the outer layers, inner layers and within the layer itself. Eq. (1) represents the two axial and azimuthal components of the magnetic field [37].

$$B_{i\theta} = \mu_0 \left(\frac{1}{2\pi r_{ip}} \sum_{k=1}^{i-1} \alpha_k I_k + \left(\frac{r_{ip}^2 - r_{ii}^2}{r_{io}^2 - r_{ii}^2} \right) \frac{I_i}{2\pi r_{ip}} \alpha_i \right)$$

$$B_{iz} = \mu_0 \left(\sum_{k=i+1}^{2N} \alpha_k \beta_k \frac{I_k}{L_{pk}} + \left(\frac{r_{io} - r_{ip}}{r_{io} - r_{ii}} \right) \frac{I_i}{L_{pi}} \alpha_i \beta_i \right)$$

$$B_i = \sqrt{B_{i\theta}^1 + B_{iz}^2}$$
(1)

where, $B_{i\theta}$ is the azimuthal component, B_{iz} is the axial component, μ_0 is the vacuum permeability, α_i and β_i are the current direction and the direction of the tape twist in the layer, respectively, which are represented by the values of -1 and +1. r_{ii} and r_{io} represent the inner and

Table 4
Values of self and mutual inductances (mH) between layers in the circuit model.

Layer	Layer 1	Layer 2	Layer 3	Layer 4	Layer 5	Layer 6	Layer 7	Layer 8
Layer 1	0.03999	0.02972	0.07104	0.071	0.10020	0.10033	0.12801	0.128
Layer 2	0.02972	0.01133	0.04779	0.04772	0.08687	0.07708	0.10478	0.10475
Layer 3	0.07104	0.04779	0.02707	0.20455	0.05644	0.05629	0.08391	0.08393
Layer 4	0.071	0.04772	0.20455	0.20455	0.03455	0.03151	0.06215	0.06215
Layer 5	0.10020	0.08687	0.05644	0.03455	0.92526	0.01489	0.04254	0.04254
Layer 6	0.10033	0.07708	0.05629	0.03151	01,489	0.00583	0.03202	0.03210
Layer 7	0.12801	0.10478	0.08391	0.06215	0.04254	0.03202	0.05033	0.01753
Layer 8	0.128	0.10475	0.08393	0.06215	0.04254	0.03210	0.01753	0.00766

outer radius of each layer, r_{ip} is the distance from the axis to the center of the tape, and L_{pi} is the length of the twist pitch of each layer. Considering the tape structure, the axial and directional components can be divided into parallel components $B_{i\mid i}$ and longitudinal components $B_{i\perp}$ according to Eq. (2).

$$\begin{array}{l} B_{i\parallel} = B_{iz} Sin(\alpha_i) - B_{i\theta} Cos(\alpha_i) \\ B_{i\perp} = B_{iz} Sin(\alpha_i) - B_{i\theta} Cos(\alpha_i) \end{array} \tag{2}$$

By properly determining the current directions and the direction of the tape twist, the axial effect of the field (Biz) can be effectively eliminated. On the other hand, if the twist pitch is very small, the axial component will be zero and only the azimuthal component will exist. Considering the creation of the $B_{i\theta}$ by the inner layers during the high current transferring, this component reduces the critical current in each tape and layer. Also, for large magnetic field, the radius of the cable cannot be considered smaller than a certain value. In fact, reducing the radius of the former layer increases the directional magnetic field in the outer layers, which will seriously reduce the critical current. Therefore, it is necessary to consider a suitable structure to reduce the effect of the magnetic field in the cable [35]. Accordingly, by increasing the amplitude and changing the direction of the magnetic field, a reduction in the critical current in the HTS tape will be provided. Generally, in the low magnetic field, Eq. (3) is used to express the dependence of the critical current density on the magnetic field [32,38]:

$$J_c(B) = \frac{J_{c0}}{\left(1 + \frac{\sqrt{(kB_{\parallel})^2 + B_{\perp}^2}}{B_c}\right)^{-\alpha}}$$
(3)

Where, J_{c0} is the critical current density at the reference temperature, $\alpha=0.65,\ k=0.45$, and $B_c=20$ mT. In order to consider the effect of temperature on the critical current density, $J_{cT}(T)$ will be substituted for J_{c0} , as shown in Eq. (4).

$$J_{cT}(T) = \begin{cases} \frac{(T_c - T)^a}{(T_c - T_0)^a} J_{c0}, \ T \le T_c \\ 0, T > T_c \end{cases}$$
 (4)

where, T_0 is the reference temperature and T_c is the critical temperature [39–41]. Critical temperature and critical current are two important variables that directly affect the resistance of the superconducting tape [2]. The resistance of the HTS tape is very small under normal operating conditions and when it is within the superconducting region. However, in the transient state when the current density exceeds the critical limit, the resistive behavior of the HTS tape will change. According to Eq. (5), three regions can be presented with respect to the changes in current density.

$$ho_{PL1} = egin{cases} 0 & ext{if} \; |J| \; < \; J_c \ rac{E_0}{|J|} \left(rac{|J|}{J_c} - 1
ight)^{n_1} & ext{if} \; |J| \geq J_c \end{cases}$$

$$\rho_{PL2} = \begin{cases}
0 & \text{if } |J| < \gamma J_c \\
\frac{E_0}{|J|} \left(\frac{|J|}{J_c} - \gamma \right)^{n_2} & \text{if } |J| \ge \gamma J_c
\end{cases}$$

$$\rho_{sc} = \frac{(\rho_0 + \rho_{P11} + \rho_{P12}) \times \rho_{sat}}{\rho_0 + \rho_{P11} + \rho_{P12} + \rho_{sat}}$$
(5)

Where, ρ_0 is the resistivity of the tape in the superconducting state, ρ_{sc} is the total superconducting resistivity, $\gamma=2$, E_0 is equal to 0.1 V.cm⁻¹, n_1 =2.8 and n_2 =30 indicated the index value, and ρ_{sat} is the constant resistivity of tape in the non-superconducting state. In order to evaluate the cable under fault conditions and after its removal, it is necessary to analyze its thermal behavior in addition to examining the resistive behavior of the superconductor, which can be presented by Eq. (6).

$$DC_p(T) \frac{d_T}{d_t} = G(T, I) - Q(T, t) \left[\frac{W}{m^3} \right]$$

$$G(T,I) = rac{
ho_{
m sc}(T)I_{
m sc}(I_{
m sc}-I_{
m c}(T))}{S_{
m sc}} \left[rac{m{W}}{m{m}^3}
ight]$$

$$\rho_{sc}(T) = \rho(T_{ref})(1 + \beta(T - T_{ref})) \tag{6}$$

where, $C_p(T)$ is the specific heat coefficient, S_{sc} is the cross-sectional area of the tape, D is the density of the tape, Q is the heat dissipated, and G is the heat generated in the tape. For YBCO tape, $\rho(T_{ref})$ is the normal state resistance and $\beta=0.007~K^{-1}$ [40,42].

Another important component in the modeling are the self and mutual inductances. The self and mutual inductances of each layer are calculated based on the magnetic field energy due to the current passing through the different layers according to Eq. (7) [43,44].

$$L_{i} = \mu_{0} \left(\frac{\pi r_{i}^{2}}{L_{pi}} + \frac{\ln \left(\frac{D}{r_{i}} \right)}{2\pi} \right)$$

$$M_{ij} = \mu_{0} \left(\frac{\pi \alpha_{i} \alpha_{j} r_{i}^{2}}{L_{pi} L_{pj}} + \frac{\ln \left(\frac{D}{r_{i}} \right)}{2\pi} \right) \left(r_{i} < r_{j} \right)$$

$$(7)$$

In this relation, μ_0 is the vacuum permeability constant, r_i is the layer radius, L_p represents the layer twist pitch, D is the distance between each superconducting layer and the center of the former, and α_i and α_j are the twist directions of each layer. In addition, in order to consider the capacitance between the layers with respect to the insulation thickness, Eq. (8) can be used.

$$C_{ij} = \frac{2\pi\varepsilon_r \varepsilon_0}{\ln\left(\frac{r_i}{r_i}\right)} j > i \tag{8}$$

where, ε_0 is the dielectric constant of vacuum, ε_r is the relative dielectric constant of the insulating material, r_i is the radius of the i_{th} conductive layer, and r_j is the radius of the j_{th} conductive layer [45,46]. For better

Table 5
Capacitance values between layers in the electric circuit model.

Location of capacitor	Value (nF)
Between Layers 1 and 2	1.1816
Between Layers 2 and 3	1.3209
Between Layers 3 and 4	1.2612
Between Layers 4 and 5	1.4005
Between Layers 5 and 6	2.6436
Between Layers 6 and 7	1.8779
Between Layers 7 and 8	1.0172

understanding, the inductance and capacitance values of model have been shown according to Tables 4 and 5.

3.3. Losses in self-shielding HTS DC cable

The losses in a HTS cable include five components, namely Magnetization Losses, AC losses, dielectric losses, heat leakage losses and coolant viscosity losses. Among them, magnetization and AC losses play a very important role in the total cable losses.

3.3.1. Magnetization loss

The Magnetization Losses produced by the parallel magnetic field in the superconducting tape can be calculated as follows.

$$Q_{mi} = \begin{cases} \frac{2fB_{i}^{2}}{\mu_{0}} \times \frac{\beta_{i}S_{i}}{3}, \ \beta_{i} < 1\\ \frac{2fB_{i}^{2}}{\mu_{0}} \times \left(\frac{1}{\beta_{i}} - \frac{2}{3B_{i}^{3}}\right)S_{i}, \beta_{i} > 1 \end{cases}$$
(9)

$$B_i = \frac{B_i}{\mu_0 J_c b} \tag{10}$$

where S_i is the area of the i^{th} layer, J_c is the critical current density of a tape, b is half the thickness of the tape, and f is the frequency of the AC magnetic field. Therefore, the Magnetization Losses of the cable will be equal to the sum of the Magnetization Losses in the different layers [24]:

$$Q_m = \sum_{i=1}^{i} Q_{mi} \tag{11}$$

3.3.2. Transport current loss

The Transport Current Loss can be calculated by considering the

Norris equation. The transport current loss of layer i can be expressed using the current of that layer according to Eq. (12).

$$Q_{ti} = \frac{\mu_0 f I_{ci}^2}{2\pi} \left[(2 - F_i) + 2(1 - F_i) \ln(1 - F_i) \right]$$
 (12)

In the above equation, $F_i = \frac{I_{pi}}{I_{cl}}$, and the cable current loss is obtained from the sum of the losses in each layer. I_{ci} is the critical current of layer i, and I_{pi} is the peak value of the AC current flowing in the ith layer [24].

3.3.3. Other losses and calculation of total losses

Dielectric losses are generated in the insulation layer and can be obtained by the Eq. (13) [38,47].

$$Q_{ins} = 2\pi f C V^2 tan \delta \left[W / m \right] \tag{13}$$

where C is the capacitance of the insulating material and $\tan \delta = 6 \times 10^{-4}$ is the insulation loss coefficient. Also, the heat leakage losses along the cable and the viscosity losses of the LN2 cooling fluid can be calculated by Eqs. (14) and (15) [47]:

$$Q_{leakage} = \frac{2k\Delta T}{ln\left(\frac{D_{out}}{D_{ln}}\right)} \left[W/m\right] \tag{14}$$

$$Q_{\theta} = \frac{G\Delta P}{\rho_{LN2}} [W] \tag{15}$$

In the above equations, $k=1.5\times 10^{-4}$ [W/m] is the equivalent thermal conductivity of the thermal insulation layer, ΔT is the temperature difference between the inner and outer surfaces of the insulation, D_{out} and D_{in} are the outer and inner diameters of the cryostat, respectively, G is the fluid flow rate of 1.1 kg/s, and ΔP is the pressure change. The outlet temperature of the LN2 can be approximately calculated by Eq. (16).

$$\Delta T(i) = T_{out}(i) - T_{in}(i) = \frac{QT}{GC_n(T)} [W/m]$$
 (16)

 $C_p(T)$ is the specific heat of YBCO tape and QT is the total cable losses including AC losses, dielectric losses, heat leakage losses and the viscosity of the cooling fluid, which is calculated from Eq. (17).

$$QT = Q_{leakage} + Q_{\theta} + Q_{ins} + Q_m + Q_t$$
 (17)

3.4. Modeling the ripple effect in the cable current

In order to simulate the ripple effect produced in the DC current, the

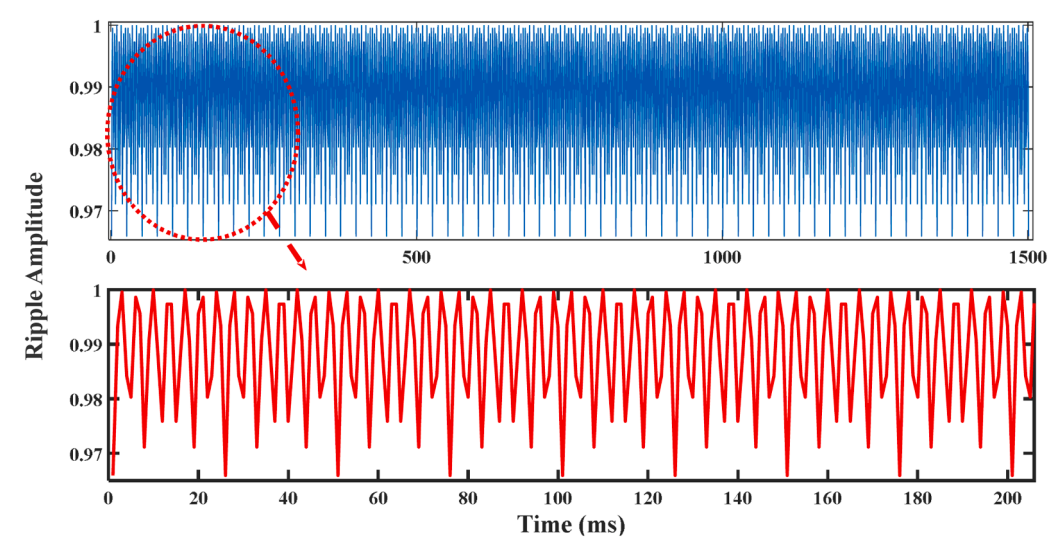


Fig. 3. Ripple current amplitude at the output of a 12-pulse rectifier.

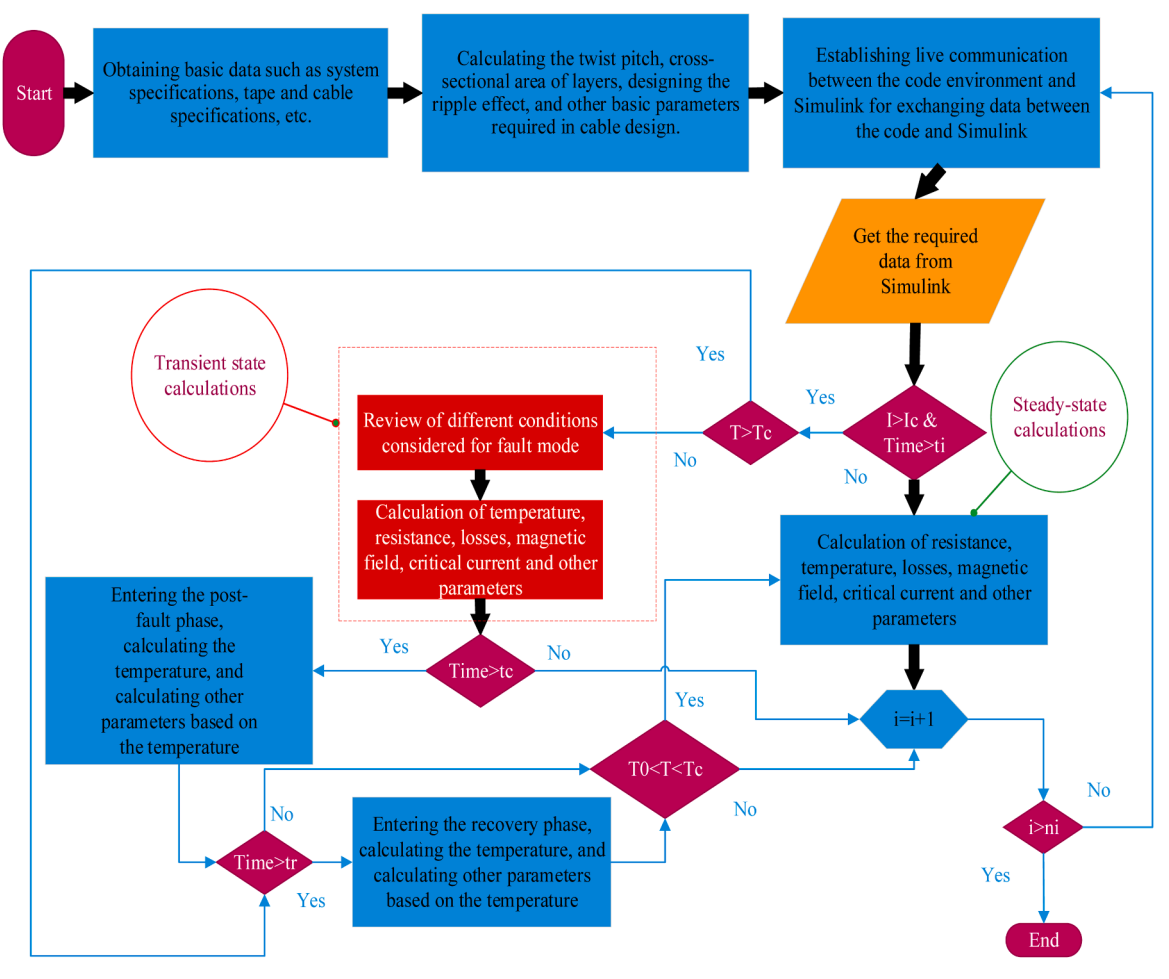


Fig. 4. Flowchart for modeling procedure of Self-shielding DC HTS Cable.

12 pulses rectifier output current is simulated, which has been shown in Fig. 3. In general, the p-pulse rectifier output current can be expressed as Eq. (18).

$$I_p(t) = \frac{\pi}{p} sin\left(\frac{\pi}{p}\right) \left[1 - \sum_{n=1}^{\infty} \frac{2}{(pn-1)(pn+1)} cos(pn\omega t)\right]$$
 (18)

where n is an integer, t is the time in seconds, p is the number of pulses,

and ω is the AC angular frequency. From the above equation, the rectified current can be obtained, including the DC current component along with the ripple current. The ratio of the ripple current to the DC current can be calculated by Eq. (19) [48,49].

$$k_p = \frac{\pi}{2p} \tan\left(\frac{\pi}{2p}\right) \tag{19}$$

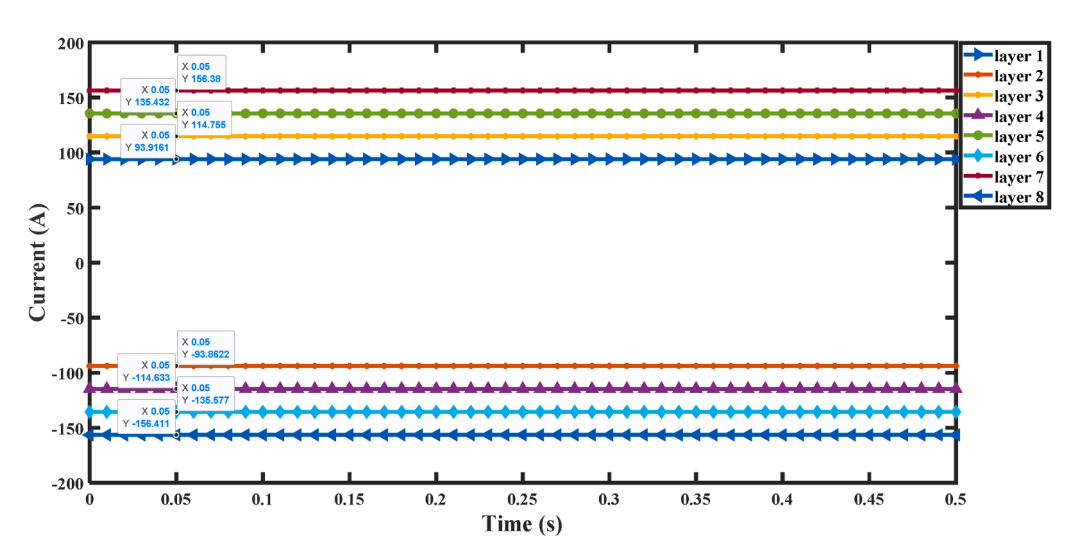


Fig. 5. Current flowing through the cable layers in steady state and without considering the AC ripple effect.

Table 6Values obtained from the simulation of the through and critical current in each layer of the cable.

Layer number	Layer 1	Layer 2	Layer 3	Layer 4	Layer 5	Layer 6	Layer 7	Layer 8
Current	93	93	114	114	135	135	156	156
layer Critical current	540	546	620	549	572	832	928	956
Nominal critical current	684	684	830	830	988	988	1140	1140

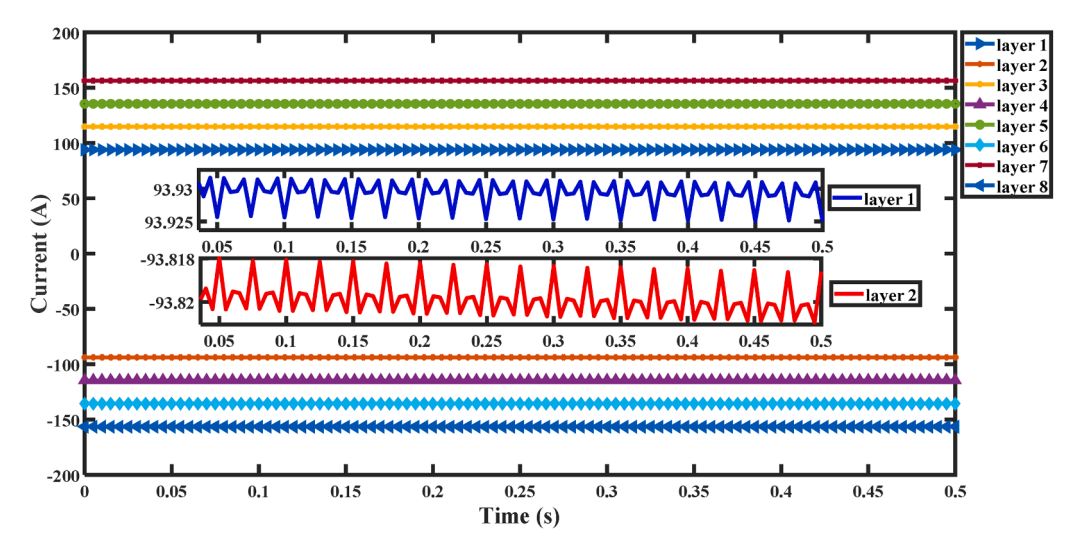


Fig. 6. Ripple effect and amplitude of current flowing through each layer of the cable in steady state.

Based on the presented formulation, Fig. 4 shows the flowchart of modeling the self-shielding DC superconducting cable under steady-state and transient operation.

4. Results and discussion

In order to analyze and evaluate the performance of the proposed model, the results are presented in two general scenarios. In the first scenario, the performance of the cable in the steady state of the power system is examined. The effect of ripple on the performance of the cable and losses is evaluated. The second scenario is based on the study of the transient state on the Self-shielding DC HTS cable. Under these conditions, the effect of the type and resistance of the fault on the cable parameters is investigated.

4.1. Stable state performance of the cable

The modeled cable is investigated in the steady state under a 500 A current and in two cases including without ripple effect and with it. Fig. 5 shows the current distribution between the cable layers in the state without ripple. As can be seen, the current distribution in the forward and backward layers is equal to each other. These conditions indicate the existence of the current balance relationship (I1 = -I2, I3 = -I4, I5 = -I6, I7 = -I8) in the modeling [43]. According to the results presented in [43], for a current of 500 A passing through the cable, the current in paths 1 to 4 is equal to 94, 108, 132, and 148 A, respectively, which are consistent with the results presented in Fig. 5 of the proposed model. Since in multilayer cables, the greatest amount of current passes through the outermost layer, as can be seen in the figure, in the presented model, the greatest current passes through layers 7 and 8.

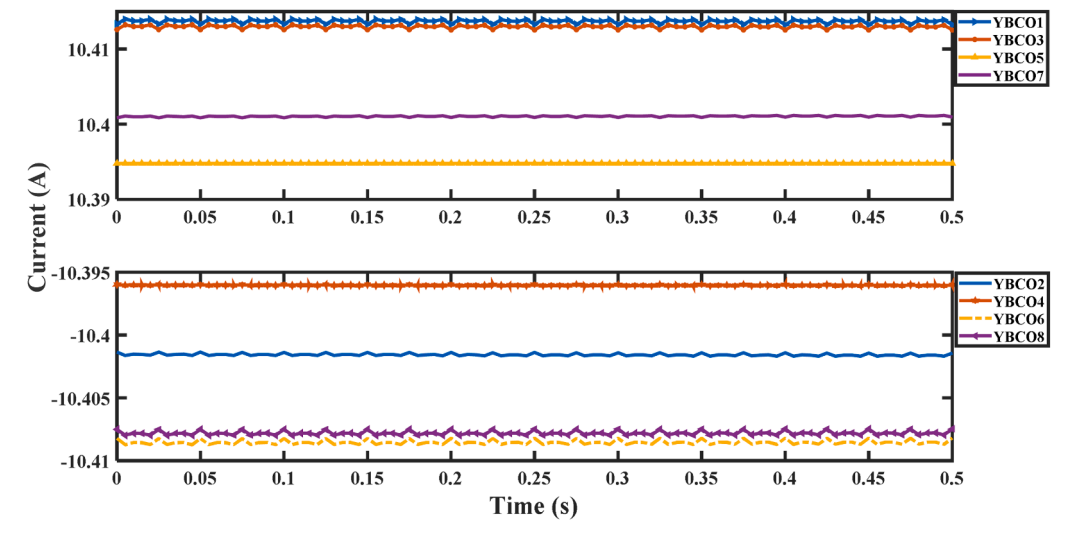


Fig. 7. Current amplitude through the YBCO layer of the superconducting tape in each cable layer in steady state with ripple effect.

Table 7

AC losses due to ripple effect in each cable layer (w/m).

Layer number	Layer 1	Layer 2	Layer 3	Layer 4	Layer 5	Layer 6	Layer 7	Layer 8
AC loss	0.367	0.370	0.516	0.453	0.565	0.814	1.053	1.079

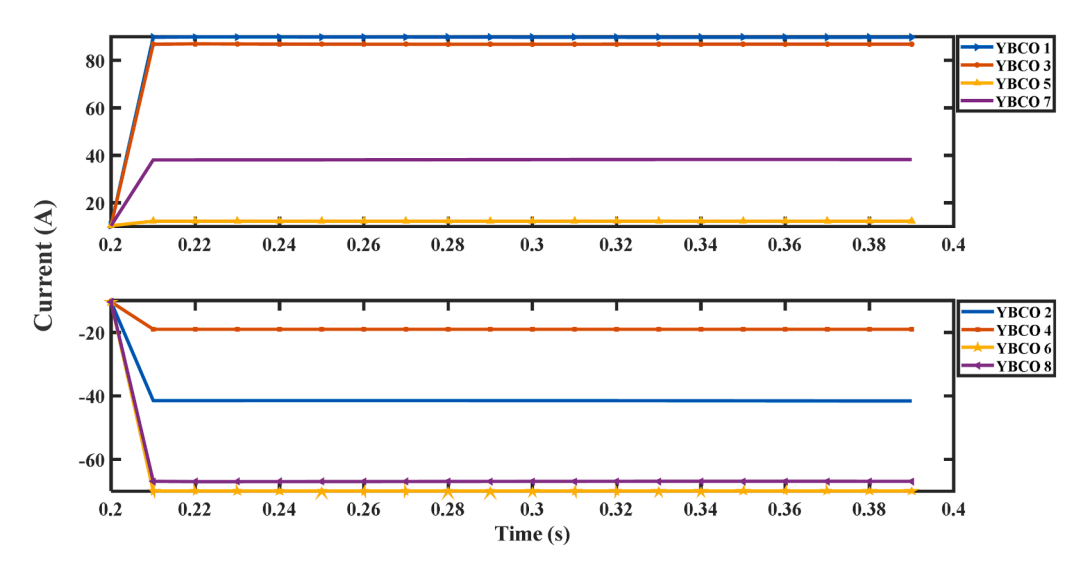


Fig. 8. YBCO layer Current in each of the cable layers during p-p fault and Rg=0.5 Ω .

Considering the critical current of each superconducting tape which is equal to 76 A, the rated critical current capacity of the cable layers will be achievable according to the number of tape in each layer. Table 6 shows the rated critical current of each layer. Due to the same current in the forward and backward layers, the rated critical current of the cable will be equal to the sum of the critical currents of the layers, which is equal to $3648 \, \text{A}$.

In order to evaluate the effect of ripple on the performance of the self-shielding DC superconducting cable, the ripple output of the 12-pulse converter is applied to the input current. Fig. 6 shows the current flowing through the different layers in this case. For greater clarity, the effect of AC ripple on the DC current amplitude in the current distribution of layers 1 and 2 is magnified.

Fig. 7 shows the current flowing through the YBCO layer in the superconducting tape in different layers. As the radius of the outer layers' increases, the number of tape increases. This condition coincides with the increase in current flowing through the outer layers and consequently leads to the same current flowing through the tape in different layers.

Under steady state operation conditions, AC losses in the absence of ripple will be zero. However, considering the ripple effect of the current in each layer, it is necessary to examine the AC losses. Table 7 shows the AC losses in each layer of the cable. In addition, under steady state operation, the specific heat coefficient of the superconducting tapes in the layers remains almost constant at 0.18 (J/gK) and the temperature of the layers is calculated in the range of 77 to 78 K.

4.2. Investigating the cable performance in transient mode

In order to analyze the transient mode, the modeled cable has been evaluated under influential factors such as the type of fault and the value

of the fault resistance. Accordingly, the results were presented to investigate the effect of two types of pole-to-ground (p-g) and pole-to-pole (p-p) faults with fault resistances (Rg) of 5, 1, 0.5 and 0.1 ohms.

In the steady state, a current with an amplitude of about 10.4 A passes uniformly through the YBCO layer of all the tapes in all the layers. However, when a fault occurs, due to the change in the resistance of the superconducting tape, the current passing through the YBCO layer of the tape is not the same and, depending on the structure of each layer, the amount of layers' current will be different. Fig. 8 shows the changes in the amplitude of the YBCO layer current of the HTS tape for each of the cable layers during the time interval of the pole-to-pole fault with a fault resistance of 0.5 Ω . As can be seen, in layers 1 and 3, the YBCO layer current exceeds the critical current of 76 A for each tape, and the current passing through the other tape is lower than the critical current. Under these conditions, and with the resulting poles current of 2502 A, the cable remains in the superconducting state. Table 8 shows the comparison of the current passing through the YBCO tape in different layers for steady states with ripple effect and fault condition with a fault resistance of 0.5 Ω .

4.2.1. Effect of fault resistance on cable transient performance

In order to investigate the effect of fault resistance on the performance of self-shielding DC HTS cable, a pole-to-pole fault with a period of 0.2 s is applied to the network at the instant of 0.2 s. Fig. 9 shows the trend of current variations in different layers under fault conditions. Under these conditions, the layer current increases and the current distribution between the layers during the fault is out of symmetry between the forward and backward layers. Although the occurrence of a fault disrupts the current distribution between the layers, the total current flowing through the layers will remain the same.

The results of the fault resistance effect on the current of layers have

Table 8Comparison of the current amplitude through the YBCO layer of the HTS tape.

Layer number	YBCO 1	YBCO 2	YBCO 3	YBCO 4	YBCO 5	YBCO 6	YBCO 7	YBCO 8
In steady state with ripple	10.4139	-10.4016	10.4132	-10.396	10.3948	-10.4087	10.4011	-10.408
In p-p fault with Rg=0.5 Ω	89.84	-41.47	86.89	-19.04	12.34	-69.98	38.13	-66.96

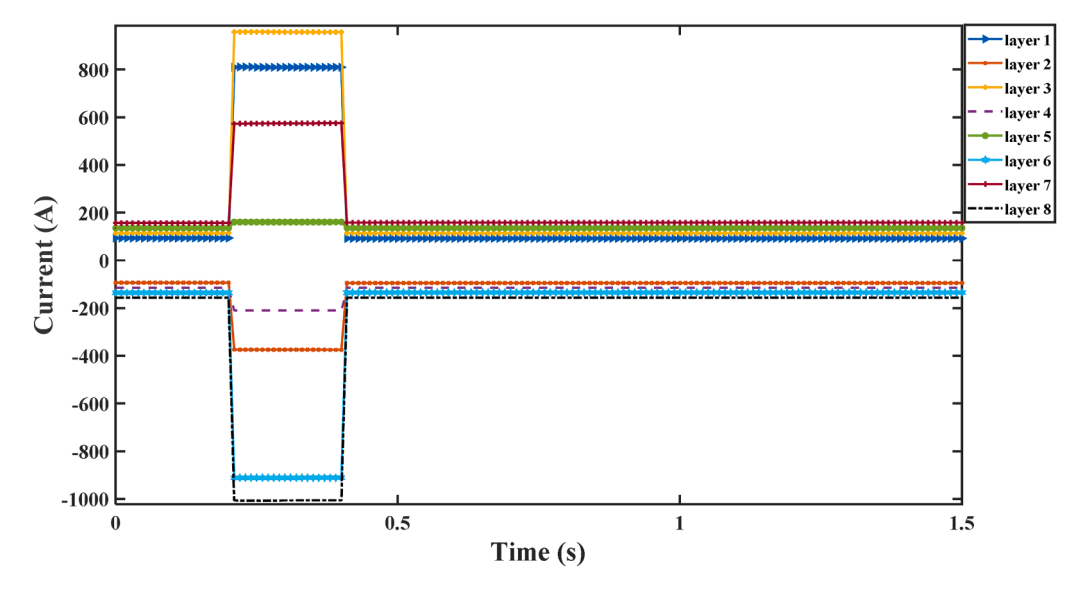


Fig. 9. Current distribution between cable layers during p-p fault and Rg= 0.5Ω .

Table 9Amplitude of current passing through different layers for a change in pole-to-pole fault resistance.

Fault resistance	Layer 1	Layer 2	Layer 3	Layer 4	Layer 5	Layer 6	Layer 7	Layer 8
5	165.56	121.85	199.09	124.14	137.97	213.17	198.21	241.42
1	452.1	234.01	536.3	162.27	148.19	523.41	365.65	518.28
0.5	810.27	374.2	957.81	209.95	160.97	911.21	574.96	1006.96
0.1	3675.64	1495.72	4329.84	591.31	263.2	4013.63	2249.42	4404.64

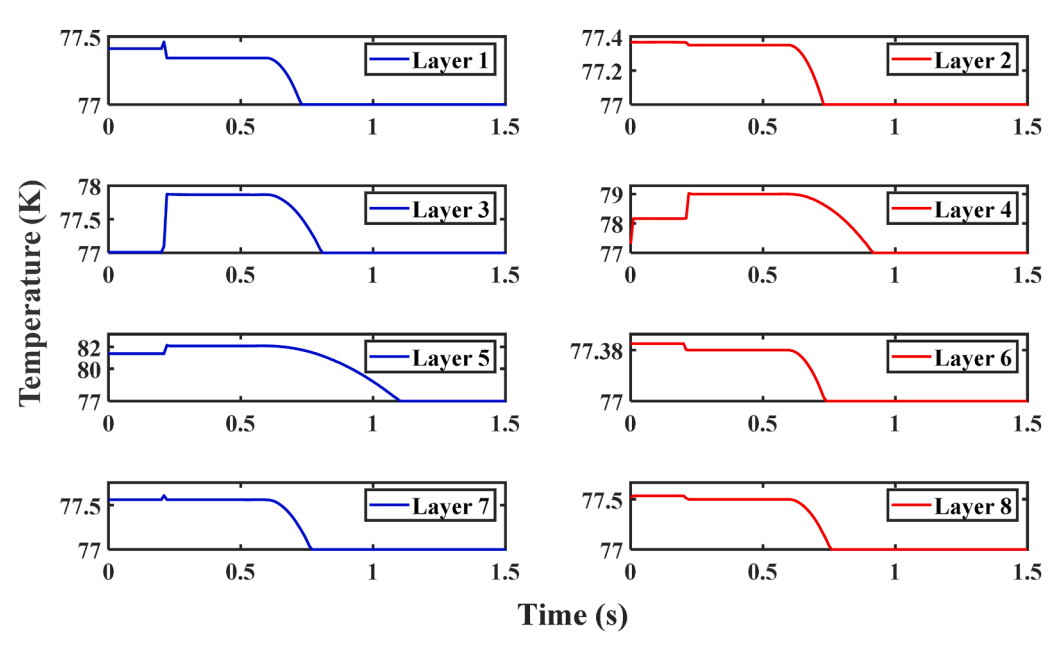


Fig. 10. Temperature variations in cable layers with p-p fault and Rg=1 Ω .

been shown in Table 9. The results show that the tapes current at Rg= 1Ω and 5Ω is less than the critical current of the tape and their performance will be in the superconducting region. While for a fault resistance of 0.5Ω , the tapes current in layers 1 and 3 are 89 and 86 A respectively, which exceeds the critical current value. Due to the interaction of the layers on each other, the resultant current of forward and backward layers reaches 2.5 kA, which is less than the rated critical current and as a result, the cable's performance will remain in the superconducting region. If the fault resistance is reduced to 0.1Ω , the amplitude of the

current will exceed the rated critical current and the cable will enter the resistive mode, so-called quench. In general, under these conditions, only the current of layers 4 and 5 will be less than the critical value, and a current in the range of 100 to 400 A will pass through the tapes of the other layers, which will be damaged if proper protection is not taken into account.

As the fault occurs and the fault current increases, the temperature in the cable layers will also change and will exceed its steady state value. At fault resistances of 5Ω and 1Ω , the temperature in the layers is very close

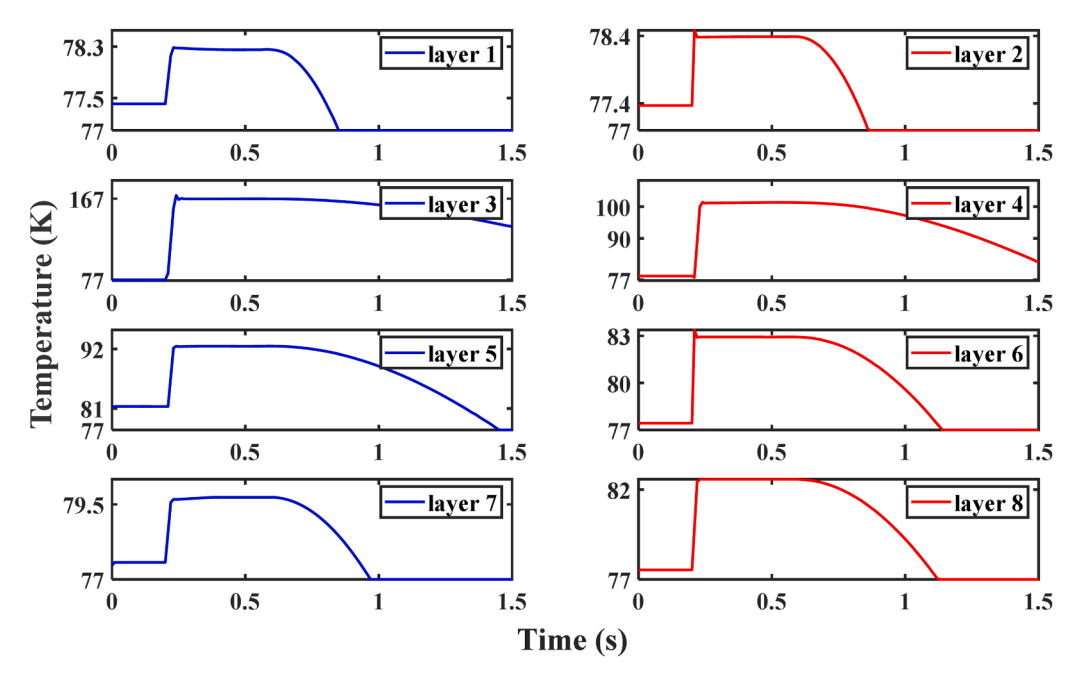


Fig. 11. Temperature variations in cable layers with p-p fault and Rg=0.1Ω.

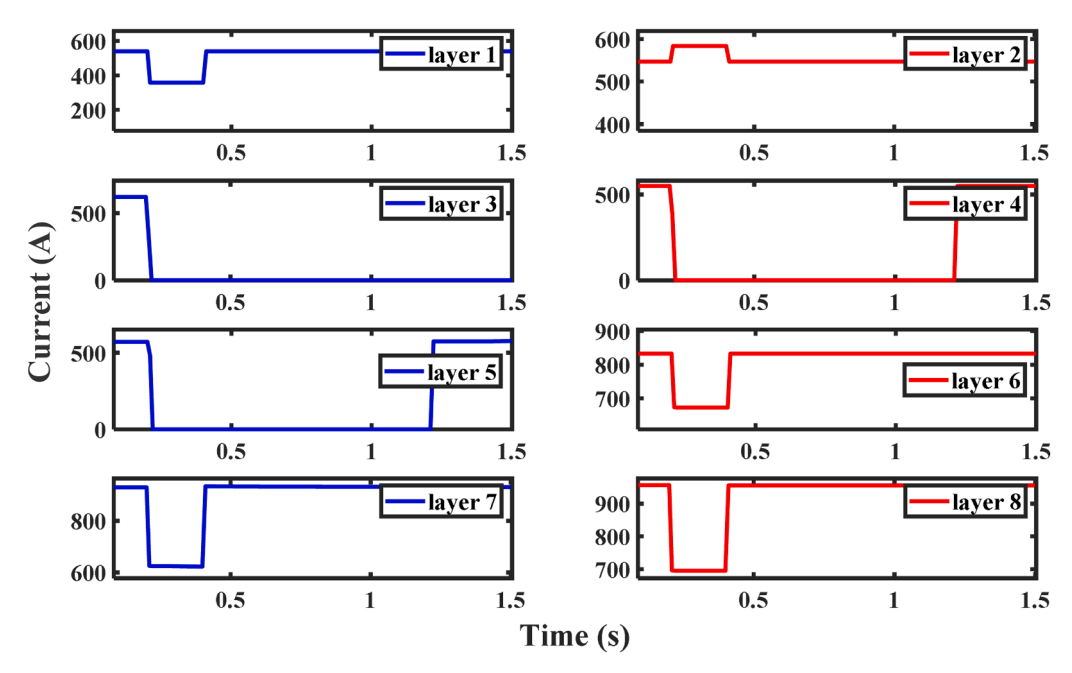


Fig. 12. Variation of cable layers' critical current during p-p fault with $Rg=0.1\Omega$.

to the steady state of the cable due to the fault current being lower than the critical current. However, by reducing the Rg to 0.5 Ω , the temperature in the central layers 3, 4, and 5 increases to 79, 80, and 82 K, respectively. At a fault with a resistance of 0.1 Ω , the temperature of these layers will be 166, 107, and 94 K, respectively. It is also observed that layers 3 and 4 will need more time to recover their thermal properties and return to the reference temperature. In this regard, the temperature variations in cable layers with p-p fault and Rg=1 Ω and Rg=0.1 Ω have been shown in Figs. 10 and 11, respectively.

One of the most important consequences of increasing temperature is the reduction of critical current. As the temperature exceeds the critical value, the critical current of the layer will become zero. Fig. 12 shows the changes in the critical current of the cable layers during a pole-to-pole fault with a fault resistance of 0.1Ω . As can be seen, in layers 3, 4

and 5 where the temperature has exceeded its critical value, the critical current in these layers have become zero. In general, temperature variations in some layers cause changes in their critical current, which can alteration the operating mode of the Self-shielding DC HTS cable.

Each tape of HTS cable will be exposed to magnetic fields generated by currents flowing through the other tapes and layers of the cable. Under fault and non-uniform current conditions, the magnetic field increases, which has a direct effect on the increase in losses. The variation of AC and Magnetization Losses under fault conditions are shown in Fig. 13.

As can be seen in these figures, the cable losses also increase with the decrease in the fault resistance, which will increase the current of layers. This condition is very severe for a fault with a resistance of 0.1Ω , and it has increased 14 times compared to Rg= 5Ω . This condition is very

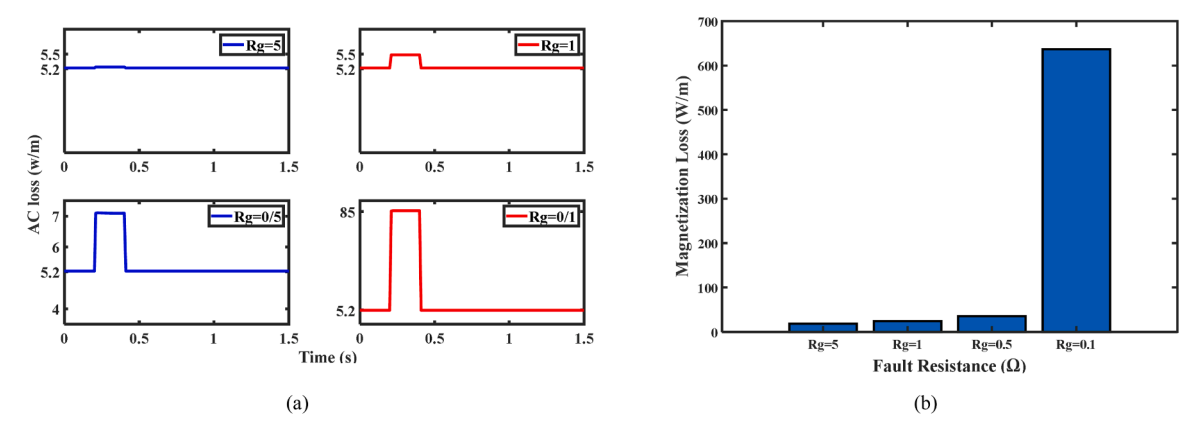


Fig. 13. Variation of studied cable losses during p-p faults with different fault resistances. (a): AC losses, (b): Magnetization Losses.

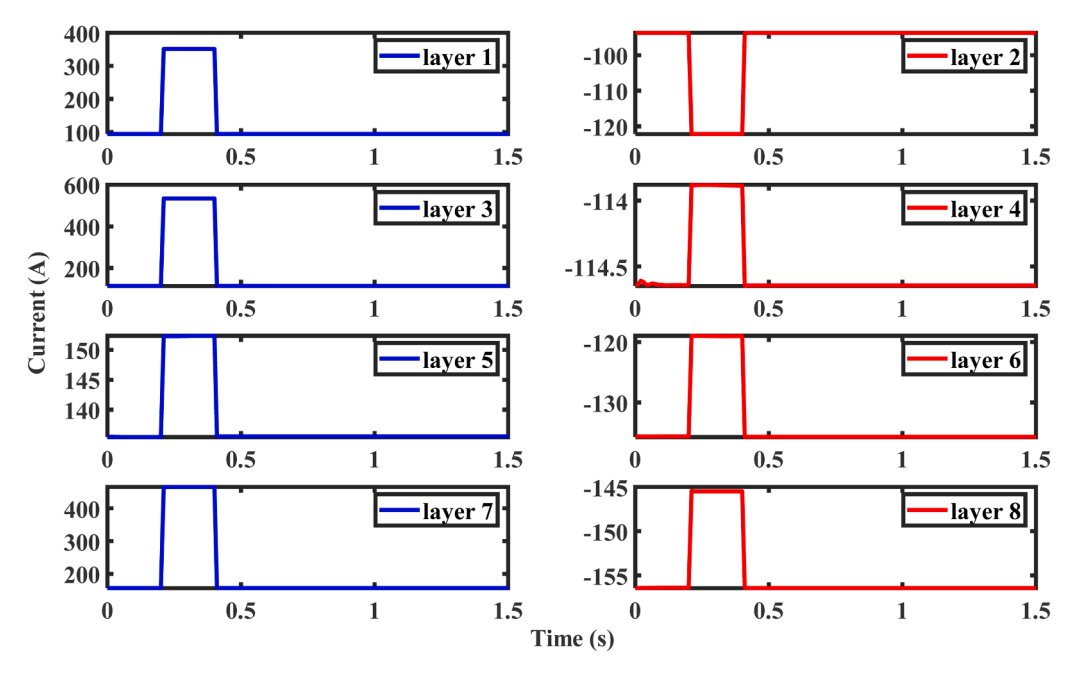


Fig. 14. Current flowing through the cable layers for p-g fault and Rg= 1Ω .

effective in terms of temperature and will change the operating mode of the cable. In addition, with increasing fault current, Magnetization Losses also increase due to the rise in the magnetic field in each layer. The growth of Magnetization Losses per change in fault resistance in Fig. (11-b) illustrates this fact.

4.2.2. Investigating the cable performance during a pole-to-ground fault

In order to investigate the effect of fault type, a pole-to-ground fault was applied to the system with the same timing as the previous case on the positive pole. The layers current and temperature were extracted in this case. As shown in Fig. 14 and 15 with different Rg, in p-g fault, the fault current passes only through layers 1, 3, 5 and 7 as the forward layers and therefore the current amplitude in these layers' increases.

The total current in the forward layers is equal to the maximum fault current and on the other hand, the total current in the backward layers is equal to the rated cable current, which remains within the load current limit. The results show that the current in p-g fault with Rg equal to 5, 1 and 0.5Ω is less than the rated critical current and the cable will remain in its superconducting operating conditions. While, the fault resistance of 0.1Ω increases the current of layers to values exceeding the critical current. For more investigation, the temperature of the layers in this case is shown in Fig. 16. As can be seen, the highest temperatures create

in layers 3, 5 and 7, which are 167, 98.2 and 97.2 K, respectively. These conditions have increased the recovery time in these layers.

In order to compare pole-to-pole and pole-to-ground fault conditions at different fault resistances, Fig. 17 and Table 10 show the maximum values of fault current of the layers. In order to better visualize the results, the critical current of each layer at the midpoint of the fault time is also presented in parentheses in Table 10. As can be seen, the highest fault current, which is equal to 4404.64 A, appears in layer 8 during pole-to-pole fault with 0.1Ω fault resistance and the lowest fault current (121.85 A) appears in layer 2 during pole-to-pole fault and 5Ω fault resistance. The results have shown that in layers 4 and 5, the fault current is lower than other layers. In fact, due to the larger inductance of these two layers compared to other layers, their magnetic field is reduced and a smaller fault current passes through them.

5. Conclusion

The self-shielding DC HTS cable has been considered in this article due to its advantages such as reduced magnetic field effect in cable layers, high current capacity at low voltage levels, no need for high voltage insulation system and no need for former layer. Based on the analysis and evaluation of steady and transient state of the self-shielding

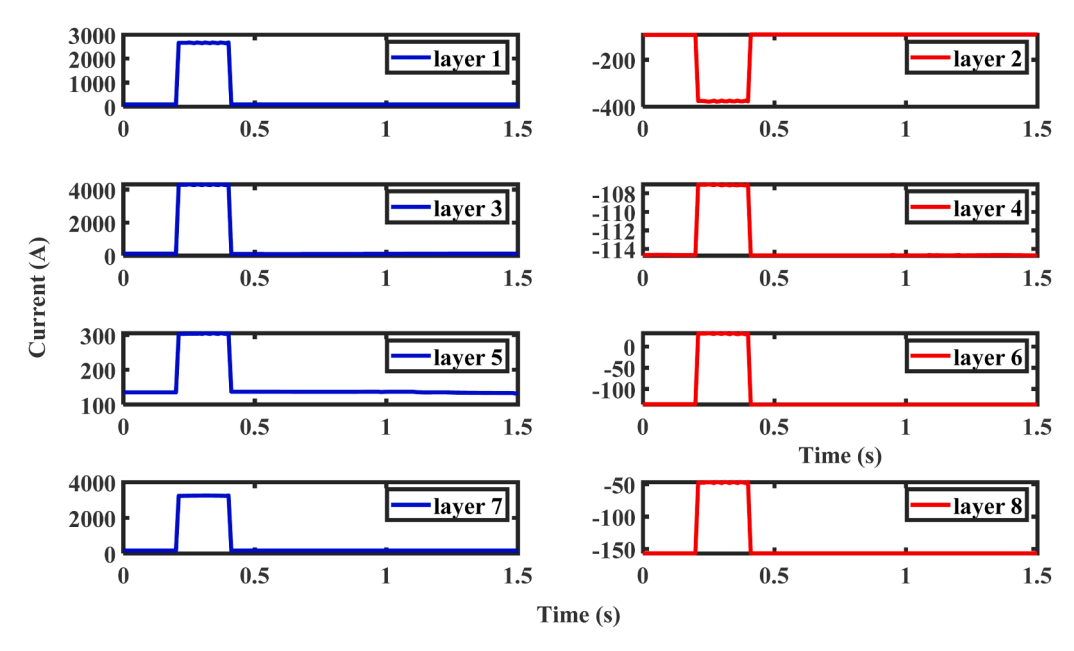


Fig. 15. Current flowing through the cable layers for p-g fault and Rg=0.1 Ω .

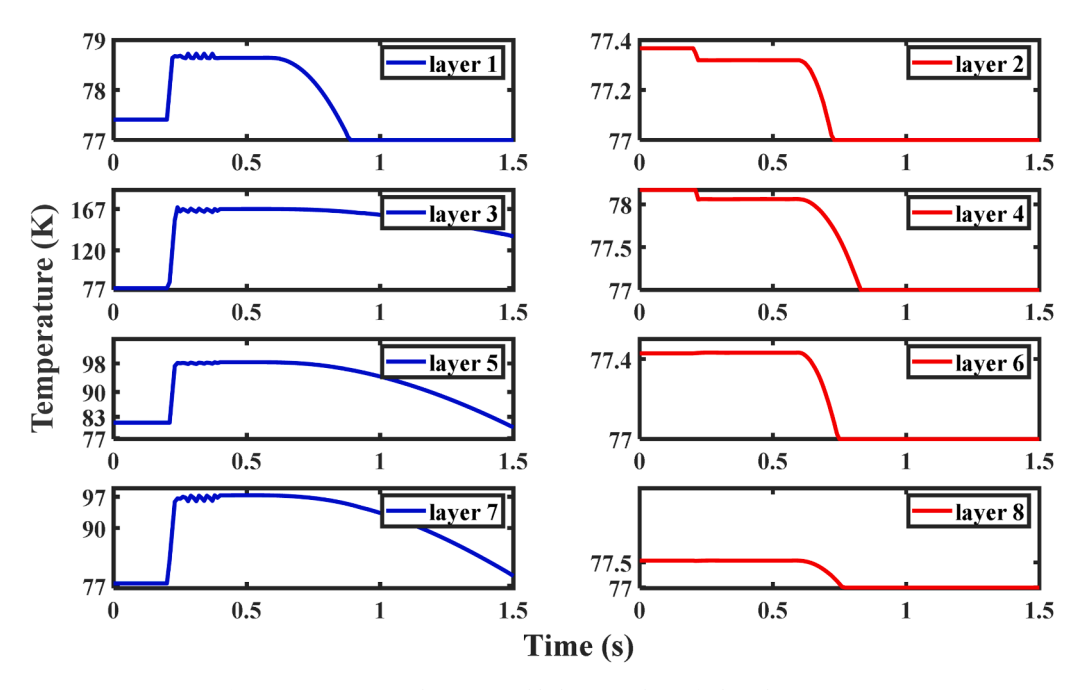


Fig. 16. Temperature changes in cable layers with p-g fault and Rg= $0.1\Omega_{\cdot}$

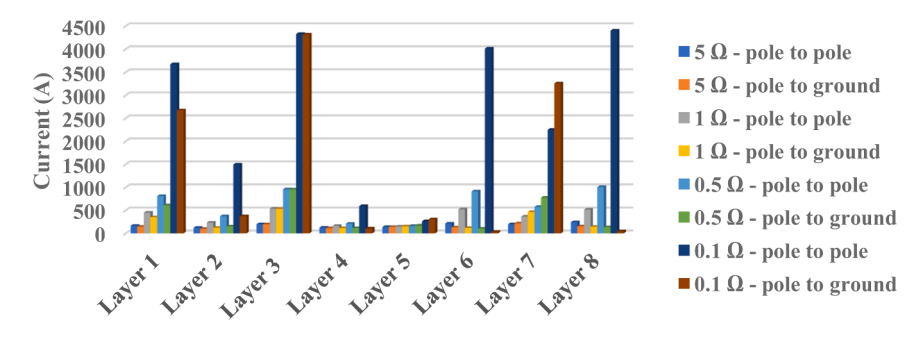


Fig. 17. Compression of fault current at different layers and fault resistances for pole-to-pole and pole-to-ground faults.

Table 10

The amplitude of fault current and critical current in the Fault time at different layers and fault resistances and type.

Fault Resistance (Ω)	Fault type	Layer 1	Layer 2	Layer 3	Layer 4	Layer 5	Layer 6	Layer 7	Layer 8
5	p-p	165.56	121.85	199.09	124.14	137.97	213.17	198.21	241.42 (966.84)
		(550.29)	(548.28)	(605.13)	(544.92)	(570.48)	(831.04)	(945.31)	
	p-g	145.28	99.47 (547.37)	198.55	114.48	138.82	132.29	218.12	154.21 (955.71)
		(547.81)		(605.49)	(550.05)	(569.75)	(832.54)	(953.24)	
1	p-p	452.1 (591.57)	234.01	536.3	162.27	148.19	523.41	365.65	518.28 (1005.4)
			(554.42)	(551.81)	(526.05)	(561.77)	(822.69)	(1016.98)	
	p-g	350.77	122.07	533.71	113.88	152.33	118.98	465.31	145.49 (954.89)
		(576.84)	(548.31)	(552.2)	(550.30)	(558.34)	(832.96)	(1060.7)	
0.5	p-p	810.27	374.2(562.21)	957.81	209.95	160.97	911.21	574.96	1006.96
		(625.15)		(499.46)	(504.67)	(551.33)	(808.88)	(1083.55)	(1024.60)
	p-g	608.33	150.39	953.83	113.12	169.28	102.3	775.12	134.55 (953.51)
		(612.46)	(549.87)	(499.76)	(550.70)	(544.80)	(833.27)	(1008.10)	
0.1	p-p	3675.64	1495.72	4329.84 (0)	591.31(0)	263.2(0)	4013.63	2249.42	4404.64
		(358.11)	(583.65)				(673.54)	(624.05)	(695.68)
	p-g	2672.67	374.39	4319.68(0)	107.04	305.06(0)	31.29	3258.31(0)	46.92(942.53)
		(421.23)	(561.98)		(553.93)		(835.32)		

DC HTS cable, the following results can be presented:

- > The interaction of the layers on each other weakens the magnetic field and balances the current passing through the forward and backward layers. However, in the event of a fault, the balance of current between these layers will be lost.
- ➤ In layers where a magnetic field is created with a high amplitude during a fault, the critical current is significantly reduced, which causes the material to exit the superconducting state.
- ➤ Considering the ripple effect equivalent to the performance of a 12-pulse converter in the system has increased the losses to >1 (w/m) in the outer layers of the cable, which has increased significantly compared to the steady state.
- ➤ With the decrease in fault resistance, the current of the cable and superconducting tapes has increased and exceeded the critical current limit. Under these conditions, losses have grown sharply and increased by 14 times. Accordingly, the temperature has also exceeded the critical margin, which leads to the possibility of changing the operating mode of the cable.
- > Among the Rg value studied, the temperature growth of cable layers in p-g fault is higher than in p-p fault for Rg=0.1 Ω . This condition is more severe in the outer layers. In addition, the recovery period in this case is also longer, which makes the conditions for returning to the superconducting state difficult.

CRediT authorship contribution statement

Mohammad Ali Salehi: Writing – original draft, Software, Formal analysis. Seyyedmeysam Seyyedbarzegar: Writing – review & editing, Visualization, Supervision, Methodology, Investigation, Conceptualization.

Declaration of competing interest

The authors declare that they have no known competing financial interests or personal relationships that could have appeared to influence the work reported in this paper.

Data availability

Data will be made available on request.

References

 M. Yazdani-Asrami, et al., Roadmap on artificial intelligence and big data techniques for superconductivity, Supercond. Sci. Technol. 36 (4) (2023) 043501, https://doi.org/10.1088/1361-6668/acbb34.

- [2] N. Varma Ulchi Suresh, A. Sadeghi, M. Yazdani-Asrami, Critical current parameterization of high temperature superconducting tapes: a novel approach based on fuzzy logic, Superconductivity 5 (2023) 100036, https://doi.org/ 10.1016/j.supcon.2023.100036.
- [3] M. Yazdani-Asrami, L. Fang, X. Pei, W. Song, Smart fault detection of HTS coils using artificial intelligence techniques for large-scale superconducting electric transport applications, Supercond. Sci. Technol. 36 (8) (2023) 085021, https://doi. org/10.1088/1361-6668/ace3fb.
- [4] A. Morandi, B. Gholizad, M. Stieneker, H. Stagge, R.W.D. Doncker, Technical and economical evaluation of DC high-temperature superconductor solutions for the grid connection of offshore wind parks, IEEE Trans. Appl. Superconduct. 26 (6) (2016) 1–10, https://doi.org/10.1109/TASC.2016.2591832.
- [5] A. Sadeghi, M.Y. Asrami, Multi-objective optimization for improving weight and fault characteristics of a DC HTS cable in Cryo-electric aircraft, Aerospace 9 (2022) 753, https://doi.org/10.3390/aerospace9120753.
- [6] S.A. Bonab, G. Russo, A. Morandi, M. Yazdani-Asrami, A comprehensive machine learning-based investigation for the index-value prediction of 2G HTS coated conductor tapes, Mach. Learn. Sci. Technol. 5 (2) (2024) 025040, https://doi.org/ 10.1088/2632-2153/ad45b1.
- [7] A. Sadeghi, S. Seyyedbarzegar, M. Yazdani-Asrami, Investigation on the electrothermal performance of a high-temperature superconducting cable in an Offshore wind farm integrated power system: fault and islanding conditions, IEEE Trans. Appl. Superconduct. 32 (8) (2022) 1–11, https://doi.org/10.1109/ TASC 2022 3196770
- [8] A. Morandi, HTS dc transmission and distribution: concepts, applications and benefits, Supercond. Sci. Technol. 28 (12) (2015) 123001, https://doi.org/ 10.1088/0953-2048/28/12/123001
- [9] J. Liang, Z. Chen, L. Wang, Magnetic field effect on critical current of different structural HTS DC cables, IEEE Trans. Appl. Superconduct. 29 (2) (2019) 1–3, https://doi.org/10.1109/TASC.2018.2890590.
- [10] G. Hajiri, K. Berger, R. Dorget, J. Lévêque, H. Caron, Design and modelling tools for DC HTS cables for the future railway network in France, Supercond. Sci. Technol. 35 (2) (2022) 024003, https://doi.org/10.1088/1361-6668/ac43c7.
- [11] G. Hajiri, K. Berger, R. Dorget, J. Lévêque, H. Caron, Thermal and electromagnetic design of DC HTS cables for the future French Railway network, IEEE Trans. Appl. Superconduct. 31 (5) (2021) 1–8, https://doi.org/10.1109/TASC.2021.3059598.
- [12] D. Doukas, Control of Superconducting Dc Transmission Systems and Solution of Coupled Electrothermal Superconducting Cable Model, School of Electrical and Computer Engineering, Division of Electrical Energy, ARISTOTLE UNIVERSITY OF THESSALONIKI. 2017.
- [13] A. Sadeghi, S.M. Seyyedbarzegar, M. Yazdani-Asrami, Transient analysis of a 22.9 kV/2 kA HTS cable under short circuit using equivalent circuit model considering different fault parameters, Physica C 589 (2021) 1353935, https://doi.org/10.1016/j.physc.2021.1353935.
- [14] M. Yazdani-Asrami, S. Seyyedbarzegar, A. Sadeghi, W.T.B. de Sousa, D. Kottonau, High temperature superconducting cables and their performance against short circuit faults: current development, challenges, solutions, and future trends, Supercond. Sci. Technol. 35 (8) (2022) 083002, https://doi.org/10.1088/1361-668/ac7ae2
- [15] A. Sadeghi, W. Song, M. Yazdani-Asrami, Intelligent Diagnostics of Internal Faults in High Temperature Superconducting Cables, 2024.
- [16] A. Sadeghi, S. Alipour Bonab, W. Song, M. Yazdani-Asrami, Short circuit analysis of a fault-tolerant current-limiting high temperature superconducting transformer in a power system in presence of distributed generations, Superconductivity 9 (2024) 100085, https://doi.org/10.1016/j.supcon.2024.100085.
- [17] J. Li, et al., Fault analysis for 110 kV HTS power cables, IEEE Trans. Appl. Superconduct. 24 (5) (2014) 1–5, https://doi.org/10.1109/TASC.2014.2347317.
- [18] A. Sadeghi, W. Song, M. Yazdani-Asrami, Intelligent surrogate model of a high-temperature superconducting cable for reliable energy delivery: short-circuit fault performance, Supercond. Sci. Technol. 37 (8) (2024) 085025, https://doi.org/10.1088/1361-6668/ad59d0.

- [19] M. Mahamed, M. Yazdani-Asrami, V. Behjat, A. Yazdani, M. Sharifzadeh, Impact of Perlator on the cooling liquid flow and hottest point temperature of superconducting windings in HTS transformer, Superconductivity 3 (2022) 100021, https://doi.org/10.1016/j.supcon.2022.100021.
- [20] W. Xiang, W. Yuan, L. Xu, E. Hodge, J. Fitzgerald, P. McKeever, Fault transient study of a meshed DC grid with high-temperature superconducting DC cables, IEEE Trans. Power Del. 37 (6) (2022) 5414–5424, https://doi.org/10.1109/ TPWRD.2022.3177406.
- [21] L. Ji-Kwang, C. Gueesoo, AC loss calculation of a multi-layer HTS transmission cable considering the twist of each layer, IEEE Trans. Appl. Superconduct. 11 (1) (2001) 2433–2436, https://doi.org/10.1109/77.920354.
- [22] H. Noji, AC loss of a high- superconducting power-cable conductor, Supercond. Sci. Technol. 10 (8) (1997) 552, https://doi.org/10.1088/0953-2048/10/8/004.
- [23] S.K. Olsen, C. Traeholt, A. Kuhle, O. Tonnesen, M. Daumling, J. Ostergaard, Loss and inductance investigations in a 4-layer superconducting prototype cable conductor, IEEE Trans. Appl. Superconduct. 9 (2) (1999) 833–836, https://doi. org/10.1109/77.783426.
- [24] J.-k. Lee, G. Cha, Magnetization loss calculation in superconducting power transmission cable, Cryogenics. (Guildf) 41 (3) (2001) 157–161, https://doi.org/ 10.1016/S0011-2275(01)00067-4.
- [25] W. Xiang, et al., DC fault study of a point-to-point HVDC system integrating offshore wind farm using high-temperature superconductor DC cables, IEEE Trans. Energy Convers. 37 (1) (2022) 377–388, https://doi.org/10.1109/ TEC.2021.3094308.
- [26] P. Chaganti, W. Yuan, M. Zhang, L. Xu, E. Hodge, J. Fitzgerald, Modelling of a high-temperature superconductor HVDC cable under transient conditions, IEEE Trans. Appl. Superconduct. 33 (5) (2023) 1–5, https://doi.org/10.1109/ TASC 2022 221148
- [27] J.G. Kim, M.A. Salmani, L. Graber, C.H. Kim, S.V. Pamidi, Electrical characteristics and transient analysis of HTS DC power cables for shipboard application, in: 2015 IEEE Electric Ship Technologies Symposium (ESTS), 2015, pp. 376–381, https://doi.org/10.1109/ESTS.2015.7157922, 21-24 June 2015.
- [28] Q. Zhou, Y. Yang, J. Wang, L. Wang, Analysis and methods for HTS DC cables, IEEE Trans. Appl. Superconduct. 31 (8) (2021) 1–3, https://doi.org/10.1109/ TASC 2021 3108738
- [29] J. Zhu, X. Bao, L. Guo, Z. Xia, M. Qiu, W. Yuan, Optimal design of current sharing in transmission conductors of a 110 kV/3 kA cold dielectric superconducting cable consisted of YBCO tapes, IEEE Trans. Appl. Superconduct. 23 (3) (2013), https:// doi.org/10.1109/TASC.2013.2244156, 5402505-5402505.
- [30] Y. Wang, H. Liu, H. Zhang, Y. Zheng, A conceptual design for HTS cable with large current capacity using Co-axial configurations, IEEE Trans. Appl. Superconduct. 20 (3) (2010) 1263–1267, https://doi.org/10.1109/TASC.2009.2039924.
- [31] Y. Wang, et al., Development of a high-temperature superconducting bus conductor with large current capacity, Supercond. Sci. Technol. 22 (5) (2009) 055018. https://doi.org/10.1088/0953-2048/22/5/055018.
- [32] H. Zhang, Y. Wang, J. Xue, Electromagnetic field analysis of a high current capacity DC HTS cable with self-shielding characteristic by 2-D simulation, IEEE Trans. Appl. Superconduct. 26 (7) (2016) 1–5, https://doi.org/10.1109/ TASC.2016.2590019.
- [33] Y.J. Yang, Self-protection of HTS cable in VSC-based DC power transmission system, in: 2020 IEEE International Conference on Applied Superconductivity and Electromagnetic Devices (ASEMD), 2020, pp. 1–2, https://doi.org/10.1109/ ASEMD49065.2020.9276185. 16-18 Oct. 2020.

- [34] Y. Wu, W. Song, M. Yazdani-Asrami, Advanced intelligent quench diagnostics for high temperature superconducting coils based on principal component analysis of voltage harmonic ratios and Support Vector Machine, Superconductivity 14 (2025) 100173, https://doi.org/10.1016/j.supcon.2025.100173.
- [35] H. Zhang, Y. Wang, A self-shielding DC HTS cable using coaxial configuration with large current capacity, IEEE Trans. Appl. Superconduct. 26 (7) (2016) 1–5, https://doi.org/10.1109/TASC.2016.2574339.
- [36] Y. Wang, H. Zhang, H. Chen, M. Liu, X. Yuan, W. Pi, Design and experimental research on self-shielding DC HTS cable model with large current capacity, IEEE Trans. Appl. Superconduct. 29 (5) (2019) 1–5, https://doi.org/10.1109/ TASC.2019.2906277.
- [37] L. Ji-kwang, C. Gueesoo, Magnetic field and magnetization loss calculation in an HTS transmission cable considering the axial field component of SC tape, IEEE Trans. Appl. Superconduct. 12 (1) (2002) 1624–1627, https://doi.org/10.1109/ TANS. 2002.143716
- [38] Y. Wang, Fundamental Elements of Applied Superconductivity in Electrical Engineering, Wiley, 2013.
- [39] W. Pi, Q. Wang, H. Zhang, Y. Wang, Q. Shi, Numerical study on fault current characteristics of self-shielded HTS DC cables made of REBCO tapes in parallel with stainless steel tapes, IEEE Trans. Appl. Superconduct. 34 (3) (2024) 1–7, https://doi.org/10.1109/TASC.2024.3354678.
- [40] J. Duron, F. Grilli, L. Antognazza, M. Decroux, B. Dutoit, Ø. Fischer, Finite-element modelling of YBCO fault current limiter with temperature dependent parameters, Supercond. Sci. Technol. 20 (4) (2007) 338, https://doi.org/10.1088/0953-2048/ 20.44.007
- [41] F. Grilli, F. Sirois, V. Zermeno, M. Vojenciak, Self-consistent modeling of the of HTS devices: how accurate do models really need to Be? IEEE Trans. Appl. Superconduct. 24 (2014) https://doi.org/10.1109/TASC.2014.2326925.
- [42] J. Duron, F. Grilli, B. Dutoit, S. Stavrev, Modelling the E-J relation of high-Tc superconductors in an arbitrary current range, Physica C 401 (1) (2004) 231–235, https://doi.org/10.1016/j.physc.2003.09.044.
- [43] H. Zhang, Y. Wang, C. Kan, Y. Fu, J. Xue, Effects of HTS tape arrangements on AC loss in self-shielding DC HTS cable with AC ripple current, IEEE Trans. Appl. Superconduct. 27 (4) (2017) 1–5, https://doi.org/10.1109/TASC.2016.2642142.
- [44] J. Zhu, Z. Zhang, H. Zhang, M. Zhang, M. Qiu, W. Yuan, Inductance and current distribution analysis of a prototype HTS cable, J. Phys. 507 (2) (2014) 022047, https://doi.org/10.1088/1742-6596/507/2/022047.
- [45] W. Pi, et al., Fault current characteristics of self-shielding HTS DC cable made of REBCO tapes, IEEE Trans. Appl. Superconduct. 34 (3) (2024) 1–6, https://doi.org/ 10.1109/TASC.2024.3365050.
- [46] S.K. Kim, S.K. Ha, M. Park, I.-K. Yu, S. Lee, K. Sim, Tri-axial core design of a distribution system class HTS power cable, Int. J. Control Autom. 5 (2012) 153-160
- [47] N. Hu, M. Toda, A.N. Ozcivan, T. Yagai, M. Tsuda, T. Hamajima, Fault current analysis in a tri-axial HTS cable, IEEE Trans. Appl. Superconduct. 20 (3) (2010) 1288–1291, https://doi.org/10.1109/TASC.2010.2042941.
- [48] Y. Ivanov, et al., Current imbalance and AC losses of long-distance DC HTS cable, IEEE Trans. Appl. Superconduct. 26 (7) (2016) 1–4, https://doi.org/10.1109/TASC 2016 2577600
- [49] K. Yoshitomi, et al., AC loss of ripple current in superconducting DC power transmission cable, Phys. Procedia 58 (2014) 326–329, https://doi.org/10.1016/j. phpro.2014.09.080.